Electric field determination in streamer discharges in air at atmospheric pressure

2011 Plasma Sources Sci. Technol. 20 035012

(http://iopscience.iop.org/0963-0252/20/3/035012)

Plasma Sources Sci. Technol. **20** (2011) 035012 (10pp) doi:10.1088/0963-0252/20/3/035012

Electric field determination in streamer discharges in air at atmospheric pressure

Z Bonaventura[1,2], A Bourdon[1], S Celestin[3] and V P Pasko[3]

[1] EM2C Laboratory, École Centrale Paris, UPR 288 CNRS, Grande voie des vignes, 92295 Châtenay-Malabry Cedex, France
[2] Department of Physical Electronics, Faculty of Science, Masaryk University, Kotlářská 2, 611 37 Brno, Czech Republic
[3] Communications and Space Sciences Laboratory, Department of Electrical Engineering, The Pennsylvania State University, University Park, PA 16802, USA

E-mail: zbona@physics.muni.cz

Received 24 September 2010, in final form 13 January 2011
Published 19 April 2011
Online at stacks.iop.org/PSST/20/035012

Abstract

The electric field in streamer discharges in air can be easily determined by the ratio of luminous intensities emitted by $N_2(C\,^3\Pi_u)$ and $N_2^+(B\,^2\Sigma_u^+)$ if the steady-state assumption of the emitting states is fully justified. At ground pressure, the steady-state condition is not fulfilled and it is demonstrated that its direct use to determine the local and instantaneous peak electric field in the streamer head may overestimate this field by a factor of 2. However, when spatial and time-integrated optical emissions (OEs) are considered, the reported results show that it is possible to formulate a correction factor in the framework of the steady-state approximation and to accurately determine the peak electric field in an air discharge at atmospheric pressure. A correction factor is defined as $\Gamma = E_s/E_e$, where E_e is the estimated electric field and E_s is the true peak electric field in the streamer head. It is shown that this correction stems from (i) the shift between the location of the peak electric field and the maximum excitation rate for $N_2(C\,^3\Pi_u)$ and $N_2^+(B\,^2\Sigma_u^+)$ as proposed by Naidis (2009 *Phys. Rev.* E **79** 057401) and (ii) from the cylindrical geometry of the streamers as stated by Celestin and Pasko (2010 *Geophys. Res. Lett.* **37** L07804). For instantaneous OEs integrated over the whole radiating plasma volume, a correction factor of $\Gamma \sim 1.4$ has to be used. For time-integrated OEs, the reported results show that the ratio of intensities can be used to derive the electric field in discharges if the time of integration is sufficiently long (i.e. at least longer than the longest characteristic lifetime of excited species) to have the time to collect all the light from the emitting zones of the streamer. For OEs recorded using slits (i.e. a window with a small width but a sufficiently large radial extension to contain the total radial extension of the discharge) the calculated correction factor is $\Gamma \sim 1.4$. As for OEs observed through pinholes, the reported results demonstrate that for local OEs, the Γ coefficient depends slightly on the radial position and is in a range [1.24, 1.28]. For line-integrated OEs, the radial variation of Γ is more significant and Γ is in the range [1.24, 1.38]. Finally, it is noted that the use of different sets of Einstein coefficients and quenching rates of excited states has negligible influence on the value of Γ.

(Some figures in this article are in colour only in the electronic version)

1. Introduction

Spectroscopic methods have been used for many years to determine the electric field in laboratory experiments on air discharges (Gallimberti *et al* 1974, Pancheshnyi *et al* 2000, Kozlov *et al* 2001, Starikovskaia *et al* 2010). Recently, spectroscopic diagnostics have also been used to obtain information on the electric field associated with lightning related transient luminous events (TLEs) occurring in the upper-atmosphere (e.g. Kuo *et al* 2005, 2009). In air discharges, the electric field can be derived from the emissions of the second positive system (SPS) of N_2: $C\,^3\Pi_u \rightarrow B\,^3\Pi_g$

and of the first negative system (FNS) of N_2^+: $B\,^2\Sigma_u^+ \rightarrow X\,^2\Sigma_g^+$. If the populations of the emitting states are assumed to be in steady state, the intensity ratio of the two emissions can be related to the ratio of excitation rates which is a sensitive function of the electric field. Then the intensity ratio of the SPS and FNS emissions allows us to determine the electric field in air discharges.

However, as mentioned by Naidis (2009), this method is rather accurate for spatially uniform discharge conditions, but can lead to significant errors for strongly nonuniform plasma discharges, such as streamer discharges. In a streamer, most of the ionization, excitation of species, and then of the discharge emission occurs in the streamer head. However, as shown by Naidis (2009), in a streamer head, the peak electric field is not located at the same position as the maximum excitation rate for $N_2(C\,^3\Pi_u)$ and $N_2^+(B\,^2\Sigma_u^+)$. In fact, the electric field at the position of the maximum of excitation rate is about 1.5 times less than the peak electric field. Therefore Naidis (2009) suggested applying a correction factor of ∼1.5 to the electric field derived from the intensity ratio integrated over the radiating plasma volume to find the true peak value of electric field in the streamer head. In addition to Naidis' effect, Celestin and Pasko (2010) showed that due to the radial distribution of the streamer, the highest contribution to the total radiation of the streamer comes from regions away from the axis of symmetry. For TLEs, Celestin and Pasko (2010) performed a series of simulations in order to derive the correction factor $\Gamma = E_s/E_e$ (where E_e is the estimated electric field and E_s is the actual peak electric field in the streamer head) as a function of altitude, applied reduced electric field and streamer polarity. They showed that the electric field derived from spatially integrated spectroscopy measurements over the radiating plasma volume needs to be multiplied by a correction factor $\Gamma > 1.4$ for positive streamers to obtain the true peak values of electric field. It is important to note that the Γ factor derived by Celestin and Pasko (2010) includes Naidis' effect. The correction factor derived in Celestin and Pasko (2010) is very useful for determining the peak electric field in TLEs as for streamer discharges propagating above ∼40 km altitude, the steady-state assumption of the emitting states is fully justified (Celestin and Pasko 2010) and since spatially integrated intensities of band systems over the radiating plasma volume are usually recorded.

For ground pressure experiments on streamer discharges in air, one can first question the validity of the steady-state approximation. This approximation is fully justified if $L \gg v_s\tau_l$, where L is characteristic length of field variation in the streamer head, v_s is streamer velocity and τ_l is the longest time scale of emissions. At ground pressure: $L \simeq 0.125 \times 10^{-3}$ m, $v_s \simeq 2 \times 10^5$ m s^{-1} (e.g. Liu *et al* 2007) and the characteristic lifetime of $N_2(C\,^3\Pi_u)$, the longest time scale of emission, is $\tau_l = 0.59$ ns. The product $v_s\tau_l$ is 0.118×10^{-3} m, and appears to be comparable to L. Therefore, for air streamer discharges at ground pressure, steady state is not fulfilled. In this case, the electric field can still be derived from emission intensities, but the relation between these quantities is much more complex and includes time derivatives of intensities (Kozlov *et al* 2001, Hoder *et al* 2008, 2010). Then, to determine accurately the electric field in streamer discharges in air at ground pressure, it is necessary to measure optical emissions (OEs) with high spatio-temporal resolution. So far only very few laboratories have an experimental set-up, such as the cross-correlation spectroscopy (CCS) used in Greisfwald (Kozlov *et al* 2001, Hoder *et al* 2008, 2010), to carry out such measurements. Most other authors used instead space (using diaphragms) and time-integrated OEs, (e.g. Pancheshnyi *et al* 2000, Starikovskaia *et al* 2010), jointly with the approximation of steady state to estimate the electric field in air discharges at atmospheric pressure. In Celestin and Pasko (2010), it was stated that although steady state is not valid at ground pressure, the derivation of the electric field through the simple ratio of integrated intensities over the whole radiating plasma volume can still be done.

In this paper, we discuss the influence of space and time integrations of OEs and the use of the steady-state relation between the electric field and the emission ratio on the derivation of the electric field in positive streamer discharges in air at ground pressure. As a reference, we consider a 2D positive streamer propagation in air at ground pressure and compute self-consistently the spatio-temporal distributions of OEs and electric field in the discharge. To validate the different approaches tested in this work to derive the electric field from OEs, we compare the results obtained with the electric field computed directly with the discharge code. Then we discuss the determination of a correction factor Γ to be used in experiments to derive accurately the electric field in positive streamer discharges in air at ground pressure.

2. Streamer model

In this work, we consider the propagation of a 2D axi-symmetric positive streamer discharge in air for the same configuration as in Celestin and Pasko (2010) that is shown in figure 1. The streamer is initiated by placing a Gaussian plasma cloud in a high-field region created by a small conducting sphere with high potential. The conducting sphere is immersed in a weak homogeneous electric field E_{amb} in which the streamer is propagating. Our simulations were performed for the same conditions as those considered by Celestin and Pasko (2010) at ground pressure. The potential applied to the conducting sphere is 6.5 kV and its radius is 0.1 cm. The homogeneous ambient electric field E_{amb} is established by remote planar electrodes. Celestin and Pasko (2010) have shown that the value of Γ varies only slightly with the variation of ambient electric field E_{amb} in the range between 5 and 25 kV cm^{-1}. Therefore, in this work we have considered a single value of the ambient electric field, $E_{amb} = 10$ kV cm^{-1}. To initiate the streamer, a neutral plasma cloud is placed on the axis of symmetry in the vicinity of the sphere. The cloud has a peak density of 10^{18} m^{-3} and a spherically symmetric Gaussian spatial distribution with a characteristic length scale of 10^{-4} m.

To compute the streamer propagation in air, we use drift-diffusion equations for electrons, positive and negative ions

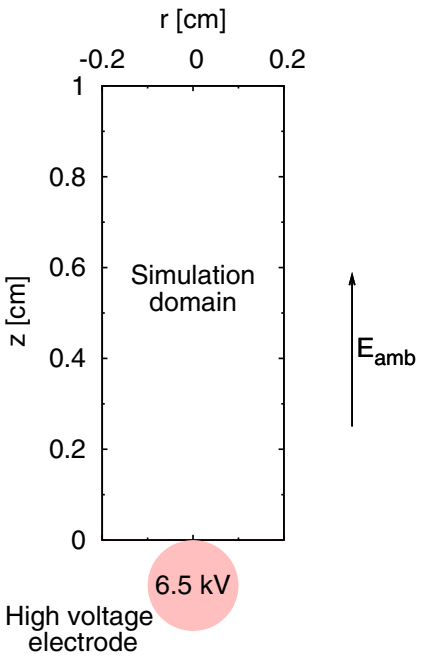

Figure 1. Simulation domain. The high voltage electrode is a conducting sphere of radius 0.1 cm that is charged to a potential of 6.5 kV. The homogeneous ambient electric field E_{amb} of 10 kV cm^{-1} is established by remote planar electrodes.

coupled with Poisson's equation (Bourdon *et al* 2007):

$$\frac{\partial n_{\mathrm{e}}}{\partial t} - \boldsymbol{\nabla}\cdot(n_{\mathrm{e}}\mu_{\mathrm{e}}\boldsymbol{E}) - \boldsymbol{\nabla}\cdot(D_{\mathrm{e}}\boldsymbol{\nabla}n_{\mathrm{e}}) = S_{\mathrm{ph}} + S_{\mathrm{e}}^{+} - S_{\mathrm{e}}^{-}, \quad (1)$$

$$\frac{\partial n_{\mathrm{p}}}{\partial t} = S_{\mathrm{ph}} + S_{\mathrm{p}}^{+} - S_{\mathrm{p}}^{-}, \quad (2)$$

$$\frac{\partial n_{n}}{\partial t} = S_{\mathrm{n}}^{+} - S_{\mathrm{n}}^{-}, \quad (3)$$

$$\boldsymbol{\nabla}^{2}V = -\frac{q_{\mathrm{e}}}{\epsilon_0}(n_{\mathrm{p}} - n_{\mathrm{n}} - n_{\mathrm{e}}), \quad (4)$$

where subscripts 'e', 'p' and 'n' refer to electrons, positive and negative ions, respectively, n_i is the number density of species i, V is the electric potential, $\boldsymbol{E} = -\boldsymbol{\nabla}V$ is the electric field, D_{e} is the diffusion coefficient of electrons, μ_{e} is the absolute value of mobility of electrons, q_{e} is the absolute value of electron charge and ϵ_0 is permittivity of free space. The S_i^{+} and S_i^{-} terms stand for the rates of production and loss of charged particles. The S_{ph} term is the rate of electron–ion pair production due to photoionization in a gas volume. The transport and source parameters are taken from Morrow and Lowke (1997). On timescales of interest for studies presented in this work, ions are assumed to be motionless. Photoionization is taken into account through the 3-Group SP_3 method derived by Bourdon *et al* (2007) with boundary conditions given in Liu *et al* (2007). The charged species transport equations are solved using the modified Scharfetter–Gummel algorithm (ISG-0) proposed by Kulikovsky (1995) with $\epsilon = 0.04$. The direct solver SuperLU (Demmel *et al* 1999a, 1999b) (http://crd.lbl.gov/~xiaoye/SuperLU/) is used to solve the finite difference form of Poisson's equation and for the photoionization source term. The direct integral solutions of Poisson's equation are used to define values of potential on the simulation domain boundaries, as in Liu and Pasko (2006). In this work, we have used a $1 \times 0.2\,\mathrm{cm}^2$ (i.e. $L_{\mathrm{d}} \times R_{\mathrm{d}}$) computational domain discretized on a fixed rectilinear grid with a mesh size of 6.2 μm and $n_z \times n_r = 1601 \times 301$ cells. To define the time step in the simulation, we use the same approach as in Bourdon *et al* (2007).

3. OEs of the discharge

To calculate the OEs of the SPS and FNS band systems, we use a model similar to the one given in e.g. Pasko *et al* (1997). The population of the excited species $N_2(C\,^3\Pi_u)$ and $N_2^+(B\,^2\Sigma_u^+)$ is governed by:

$$\frac{\partial n_k}{\partial t} = -\frac{n_k}{\tau_k} + \nu_k n_{\mathrm{e}}, \quad (5)$$

where n_k (cm^{-3}) is the population of excited state k, ν_k is the frequency of creation of excited state k by electron impact, $\tau_k = [A_k + \alpha^k_{\mathrm{N_2}} N_{\mathrm{N_2}} + \alpha^k_{\mathrm{O_2}} N_{\mathrm{O_2}}]^{-1}$ is the total lifetime of k-state, α^k_{X} is the quenching rate of state k due to collisions with molecule of type X of density N_{X} and A_k (s^{-1}) is the Einstein coefficient. To simplify notation, in the following the subscript B is used for $N_2^+(B\,^2\Sigma_u^+)$ and C for $N_2(C\,^3\Pi_u)$. All coefficients for the two band systems are taken from Liu and Pasko (2004) and are given in table 1. It is important to note that in our work, as in Liu and Pasko (2004) and Bourdon *et al* (2010), equation (5) for excited states is solved simultaneously with the streamer equations. This gives a full time-dependent solution of OEs in the modelling of the streamer processes.

The experimentally detected intensities of light for the two bands are directly proportional to the radiative deexcitation rates of $N_2(C\,^3\Pi_u)$ and $N_2^+(B\,^2\Sigma_u^+)$ (Kozlov *et al* 2001):

$$I_k = T_k A_k n_k, \quad (6)$$

where k is either $N_2(C\,^3\Pi_u)$ or $N_2^+(B\,^2\Sigma_u^+)$ and T_k is a transmission coefficient, which depends on the characteristics of the optical system and the sensitivity of the detector. In this work, we assume that the transmission coefficients T_k for the two studied band systems are equal to 1. The number of photons emitted per second from a volume element $\delta V^j = 2\pi r^j \delta z^j \delta r^j$, where r^j is the radial distance and δz^j and δr^j are the axial and radial sizes of cell j, is

$$N^j_{\mathrm{ph},k} = A_k n_k \delta V^j. \quad (7)$$

If the discharge is observed along a line of sight, the measured OE intensity (also referred to as line-integrated OE in the following) of each band system at a given time is given by

$$\Psi_k = 10^{-6} \int_{\mathcal{L}} I_k \,\mathrm{d}l, \quad (8)$$

where I_k is in cm^{-3} s^{-1}, l is in cm, the intensity Ψ_k is in Rayleighs, and the integration is performed along the optical path $\mathcal{L}$. In this paper, as in Pasko *et al* (1997) and Liu and Pasko (2004), the effects of radiative transfer between the source of the emission and the observer are not taken into account. In equation (8), the intensity, I_k, is an axially

Table 1. Einstein coefficients and quenching rates for $N_2(C\,^3\Pi_u)$ and $N_2^+(B\,^2\Sigma_u^+)$.

	α_{O_2} ($cm^3\,s^{-1}$)	α_{N_2} ($cm^3\,s^{-1}$)	A_k (s^{-1})	References
$N_2^+(B\,^2\Sigma_u^+)$	5.1×10^{-10}	2.1×10^{-10}	1.6×10^7	Pancheshnyi *et al* (2000), Paris *et al* (2005)
$N_2(C\,^3\Pi_u)$	3.0×10^{-10}	0.13×10^{-10}	2.38×10^7	Paris *et al* (2005), Pancheshnyi *et al* (1998)
$N_2^+(B^2\Sigma_u^+)$	0	4.0×10^{-10}	1.4×10^7	Liu and Pasko (2004)
$N_2(C\,^3\Pi_u)$	3.0×10^{-10}	0	2.0×10^7	Liu and Pasko (2004)
$N_2^+(B\,^2\Sigma_u^+)$	8×10^{-10}	3×10^{-10}	1.6×10^7	Valk *et al* (2010)
$N_2(C\,^3\Pi_u)$	2.9×10^{-10}	0.132×10^{-10}	2.39×10^7	Valk *et al* (2010)

symmetric function of cylindrical radius $f(r)$. Then, to calculate the intensity Ψ_k for a horizontal line of sight (namely a line perpendicular to the discharge axis), it is necessary to perform the integration in equation (8) taking into account the radial profile of I_k; this is the classical direct Abel's transformation. In this work, we define the time-integrated OEs as the intensity integrated from the time of start of the simulation to the actual time t. For example, the time-integrated local OEs are

$$\mathcal{I}_{\rm ti}(t) = \int_0^t I_k(\tau)\,{\rm d}\tau, \tag{9}$$

and line-integrated time-integrated OEs are

$$\psi_{\rm ti}(t) = \int_0^t \Psi_k(\tau)\,{\rm d}\tau. \tag{10}$$

For convenience we also define the space-averaged OEs as

$$\bar{I}_{\rm sa}(t) = 2\pi \int_0^R \int_{z_1}^{z_2} I_k(t, r, z)\, r\,{\rm d}z\,{\rm d}r, \tag{11}$$

where the radial integration goes from the axis of symmetry to a radius R and the axial integration is limited by the lower bound $z = z_1$ and upper bound $z = z_2$. Combining both, we also define time-integrated space-averaged OEs:

$$\bar{\mathcal{I}}_{\rm sati}(t) = 2\pi \int_0^R \int_{z_1}^{z_2} \int_0^t I_k(\tau, r, z)\, r\,{\rm d}\tau{\rm d}z\,{\rm d}r. \tag{12}$$

If the populations of the emitting states are assumed to be in steady state (i.e. when the time derivatives in equation (5) can be neglected), one can easily derive from equations (5) and (6) the relation between the ratio of local intensities of the two band systems and the electric field:

$$\frac{A_B \tau_B}{A_C \tau_C}\frac{I_C}{I_B} = \frac{\nu_C}{\nu_B} = \mathcal{F}(E/N), \tag{13}$$

where the dependence of $\mathcal{F}(E/N)$ on the electric field is monotonic and is given in Celestin and Pasko (2010). When the steady-state approximation is not valid (i.e. when the time derivatives in equation (5) have to be considered), a more complex relation between the intensities of the two band systems, their time derivatives and the electric field (Kozlov *et al* 2001) is obtained using equations (5) and (6):

$$\frac{A_B}{A_C}\frac{\dfrac{{\rm d}I_C}{{\rm d}t} + \dfrac{I_C}{\tau_C}}{\dfrac{{\rm d}I_B}{{\rm d}t} + \dfrac{I_B}{\tau_B}} = \frac{\nu_C}{\nu_B} = \mathcal{F}(E/N). \tag{14}$$

4. Results

4.1. Use of instantaneous spatially integrated OEs over the whole radiating plasma volume to derive the electric field

Figures 2(*a*) and (*b*) show cross sectional views of the electron density and the electric field, respectively, for a positive streamer in air at ground pressure at the moment (12.3 ns) when it crosses the middle of the simulation domain. Consistent with many previous streamer simulations, the peak electric field is located in the streamer head on the axis of symmetry of the discharge. Figures 2(*c*) and (*d*) show cross sectional views of the intensities of the SPS and FNS, respectively, integrated over a horizontal line of sight. As already observed in many previous works on air discharges at ground pressure, the most intense emission is due to the SPS. First, following Celestin and Pasko (2010), we have checked that although steady state is not valid at ground pressure, the derivation of the electric field through the simple ratio of integrated intensities over the whole radiating plasma volume can still be done. For this, instantaneous line-integrated intensities of the two bands (shown in figures 2(*c*) and (*d*)) have been integrated over the region including the streamer head and behind the head (but carefully avoiding the luminous trail close to the electrode as in Liu *et al* (2009) and Liu (2010)). The integration domain is shown with a white line in figures 2(*c*) and (*d*). From the ratio of these instantaneous spatially integrated intensities, we have derived using equation (13) a time-dependent value of the estimated electric field E_e. The ratio between the actual peak electric field in the streamer head $E_s(t)$ and the estimated field $E_e(t)$ determines the correction factor $\Gamma(t) = E_s/E_e$. Figure 3 shows the time evolution of the correction factor Γ and the peak electric field in the streamer head E_s computed from the streamer code. For the test-case studied in this work, we note that the peak electric field in the streamer head decreases smoothly during its stable propagation in the weak field region far from the spherical electrode. It is interesting to note that for $t > 8$ ns, the coefficient Γ reaches a stable value of $\sim$1.426. This value is in excellent agreement with the results obtained by Celestin and Pasko (2010). Furthermore, Celestin and Pasko (2010) observed that the value of Γ varies less than 3% over the whole range of altitudes (0–80 km) and concluded that non-similarity of streamers has no significant effect on the value of Γ. This first result shows that even though the steady state is not valid at ground pressure, the derivation of the peak electric field in the streamer can still be done using the steady-state equation (13) with instantaneous spatially integrated intensities over the whole radiating plasma volume. In Naidis (2009) a correction factor

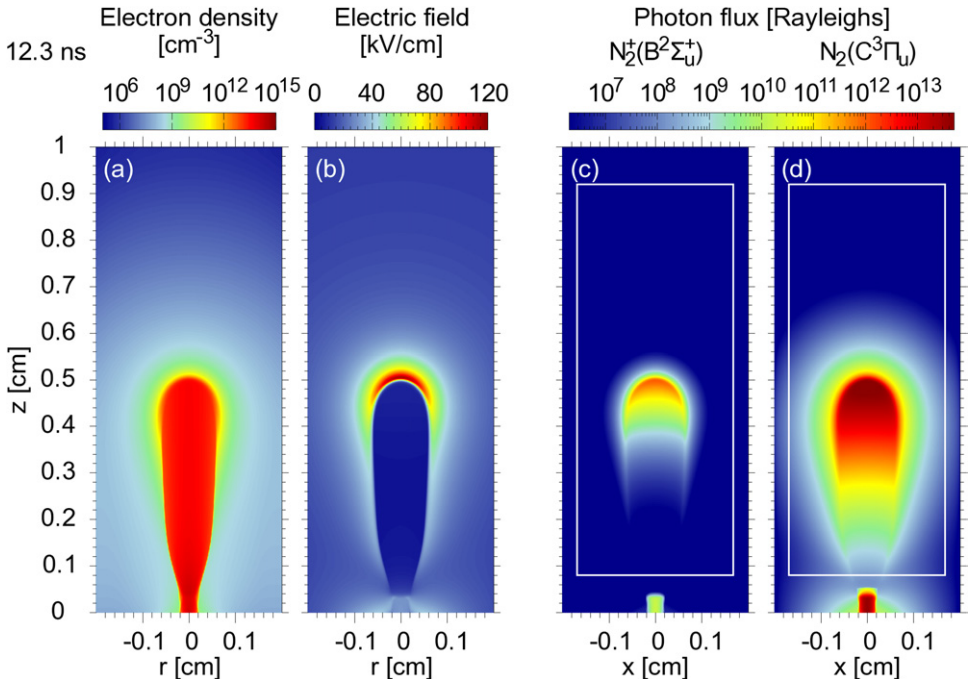

Figure 2. Cross sectional views of electron density (*a*), electric field (*b*), instantaneous flux of photons Ψ_B (*c*) and Ψ_C (*d*) emitted from $N_2^+(B\,^2\Sigma_u^+)$ and $N_2(C\,^3\Pi_u)$, respectively, for a horizontal line of sight for a positive streamer at time $t = 12.3$ ns when the streamer crosses the middle of the simulation domain. The white line in (*c*) and (*d*) represents the integration window for the volume integration of instantaneous OEs.

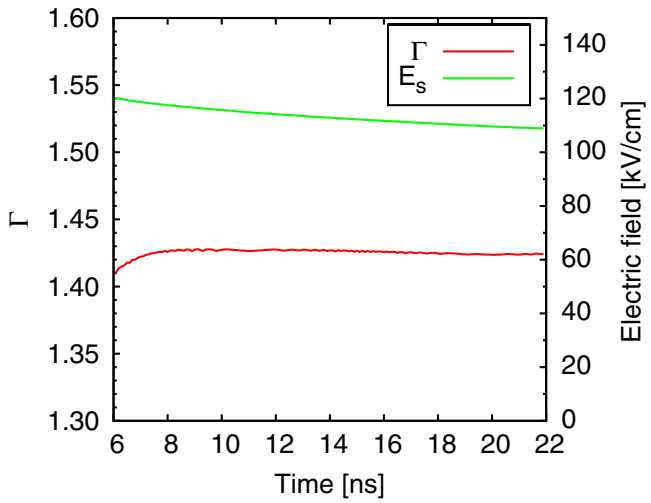

Figure 3. Time evolution of the streamer head peak electric field E_s computed with the streamer code and of the correction factor $\Gamma = E_s/E_e$, based on the electric field E_e derived from the steady-state equation (13) using instantaneous spatially integrated OEs over the whole radiating plasma volume defined in figures 2(*c*) and (*d*).

is proposed to take into account the axial dependence of the streamer characteristics. In addition to Naidis' effect, Celestin and Pasko (2010) showed that due to the dependence of streamer parameters on radial coordinate, the highest contribution to the total radiation of the streamer comes from regions away from the axis of symmetry. In order to quantify the importance of the radial dependence of the discharge on the value of Γ, figure 4 shows radial distributions of different streamer characteristics. The bottom figure presents the instantaneous SPS intensity integrated over a line of sight parallel to the discharge axis (i.e. the bottom figure corresponds to a top view of the streamer) for the integration window defined in figures 2(*c*) and (*d*). The top figure presents the radial distribution of the maximum electric field E_{max} at time $t = 12.3$ ns inside the integration window and the radial distribution of the total number of photons of the SPS emitted at time $t = 12.3$ ns per ring of thickness $\delta r^j = 6.2\,\mu$m (i.e. the radial cell size) and integrated over the axial extension of the integration window (defined in figures 2(*c*) and (*d*)). As already shown in figures 2(*b*) and (*d*), the electric field and the photon flux of SPS have their maxima on the discharge axis. Conversely, the number of photons of the SPS emitted per ring is small for small values of r as the ring surface tends to 0 for $r \to 0$ and figure 4 shows that the number of photons has a maximum at a certain distance from the axis of symmetry. Each ring *a*–*d* in figure 4 contains 25% of the total number of photons emitted from the integration window by $N_2(C\,^3\Pi_u)$. It is interesting to note that 50% of the total number of photons is emitted from regions away from the axis of symmetry (regions *c* and *d*), where the electric field is at least 10% less than the peak electric field. In agreement with Celestin and Pasko (2010), we note that because of the radial distribution of the streamer, the highest contribution to the total number of photons originates from regions away from the axis of symmetry. In addition to Naidis' effect, this results in a reduction of E_e by at least 10%, and a corresponding increase of Γ by ∼25%.

4.2. Use of time-integrated OEs spatially integrated over slits to derive the electric field

In different experiments (e.g. Pancheshnyi *et al* 2000, Starikovskaia *et al* 2010), time-integrated OEs spatially

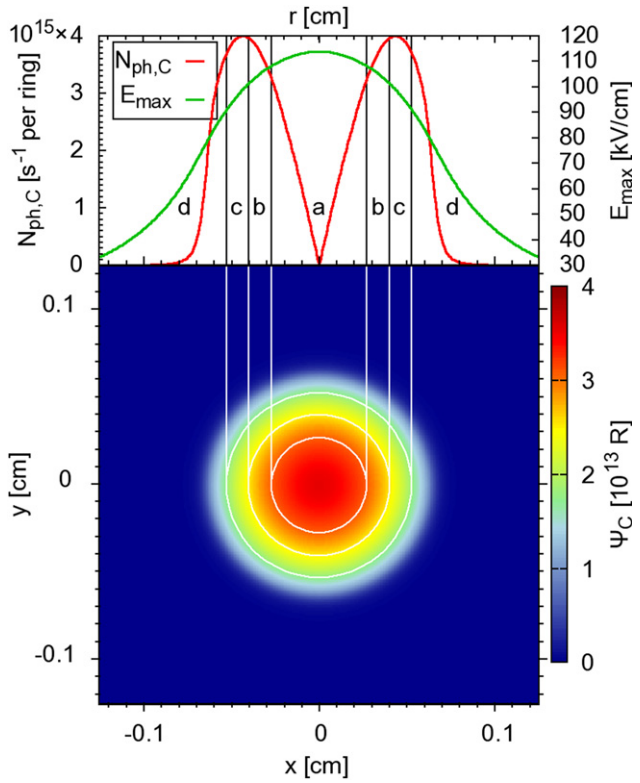

Figure 4. Radial distribution of the streamer characteristics at time $t = 12.3$ ns. Bottom: photon flux Ψ_C of $N_2(C\,^3\Pi_u)$ integrated over a line of sight parallel to the discharge axis for the integration window defined in figures 2(*c*) and (*d*). Top: radial distribution of maximum intensity of the electric field E_{max} in the integration window and radial distribution of the total number of photons $N_{ph,C}$ emitted from $N_2(C\,^3\Pi_u)$ per second and per ring of thickness $\delta r = 6.2\,\mu$m and integrated over the axial extension of the integration window. Each ring a to d contains 25% of the total number of photons emitted per second from the integration window.

integrated over diaphragms installed on the discharge axis are used together with the steady-state approximation to estimate the electric field in air discharges at atmospheric pressure. In this section, we have performed series of computations to investigate the influence of spatial integration over slits of different sizes of instantaneous and time-integrated OEs to derive the electric field in air discharges at atmospheric pressure. As a reference position we have chosen the middle of the computational domain ($z = L_d/2$), where (i) the streamer is already well developed and (ii) there still remains a sufficiently long time of propagation to perform time integration before the streamer exits from the computational domain. First, as in experiments, we have considered slits that can contain the full radial extension of the streamer (i.e. slits with a radial extension equal to radius R_d of the computational domain). It is interesting to note that in this case the results can be easily compared with these obtained using instantaneous OEs spatially integrated over the whole radiating plasma volume. Indeed, the time integration of OEs over a slit can be considered as a scanning of the entire streamer head along the streamer propagation, as the streamer head moves through the field of view of the slit. The use of such slits allows us to determine locally (i.e. along the direction of the propagation of the streamer) the peak electric field in the discharge.

In order to study the influence of the width of the slit on the derivation of the electric field, figure 5 presents the results obtained for three slit widths: $w = 0.125$, 1.0 and 2 mm. Figures 5(*a*)–(*c*) show the instantaneous peak electric field E_{max} computed with the streamer code in the window of the field of view of the different slits. The high plateau value of E_{max} corresponds to the moments of time when the streamer head is present in the slit. Then, the value of the electric field at the plateau is the peak electric field E_s. As expected, the duration of the high plateau value increases with the increase in the width of the slit. Figures 5(*a*)–(*c*) present also the time evolution of the electric field derived using the steady-state equation (13) and time-integrated OEs spatially integrated over the slits according to equation (12) as follows:

$$\bar{\mathcal{I}}_{sati}(t) = 2\pi \int_0^{R_d} \int_{L_d/2-w/2}^{L_d/2+w/2} \int_0^t I_k(\tau, r, z)\, r\, d\tau dz\, dr. \qquad (15)$$

We note that for the three slits the estimated electric field can be either higher or less than the true peak electric field E_s. The open circles in figure 5(*a*)–(*c*) show the times t for which the electric field estimated from time-integrated OEs spatially integrated over the slit is equal to the peak electric field E_s (i.e. $\Gamma = 1$). It is interesting to note that whatever the width of the slit, the estimated electric field converges towards the same value for all slits for a sufficiently high value of the upper bound of the integration in time. The converged value of the derived electric field is E_e and is less than E_s, then $\Gamma > 1$. It is important to note that the results of the time integration are not sensitive to the value of the lower time bound t_{lb} (namely in equations (12) and (15), $t_{lb} = 0$) in the integration as long as t_{lb} is less than the time of arrival of the streamer head in the slit. Figures 5(*a*)–(*c*) show that in order to derive useful information from time-integrated OEs spatially integrated over slits, the upper bound of the time integration needs to be long enough to collect all the light from the excited species created during the high plateau of electric field in the slit. For figures 5(*a*)–(*c*), the correction factor $\Gamma = E_s/E_e$ is 1.457 which is 2% higher than the one derived from instantaneous volume averaged OEs (figure 3).

The convergence of the time integration for a slit of very small width (6 μm in this case) is presented in figure 6. Due to the very small width of the slit, there is no plateau of the electric field, but simply a peak of the electric field corresponding to the peak electric field E_s in the streamer head. The time-integrated OEs spatially integrated over the slit (equation (15)) are used with the steady-state equation (13) to calculate the time evolution of the Γ coefficient. About 1 ns after the peak electric field, Γ reaches the value of 1 and increases to reach a converged value ($\Gamma > 1$) after ~6 ns, which is approximately ten times the lifetime of state $N_2(C\,^3\Pi_u)$ (0.59 ns). The resulting Γ is 1.459 which is 2% higher than the one derived from instantaneous volume averaged OEs (figure 3).

4.3. Use of instantaneous and time-integrated local and line-integrated OEs to derive the electric field

So far we have considered slits that contain the total radial extension of the streamer. In principle, in laboratory

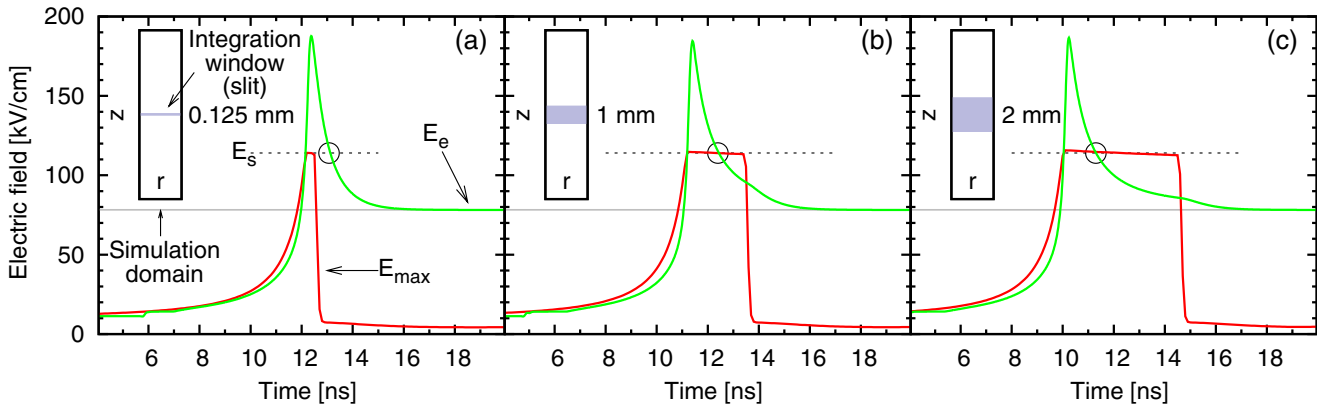

Figure 5. Estimation of the peak electric field for slits of different widths. (*a*) 0.125 mm, (*b*) 1.0 mm and (*c*) 2 mm. Red solid line: time-dependent maximum electric field E_{max} in the field of view of the slit, computed with the discharge code. E_s is the actual peak electric field of the streamer head. Green solid line: electric field derived using time-integrated OEs spatially integrated over the slits (equation (15)) in the steady-state equation (13). E_e is the converged value of the estimated value of electric field. The open circles show the time t for which the estimated electric field is equal to E_s ($\Gamma = 1$).

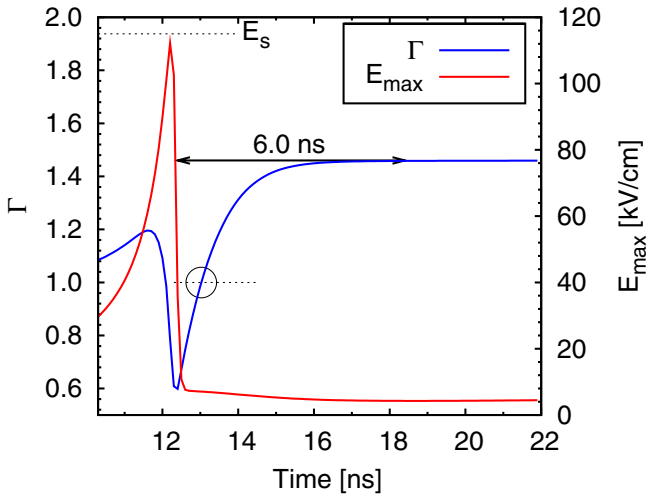

Figure 6. Estimation of the peak electric field for a slit with a width of 6 μm. Red solid line: time-dependent maximum electric field E_{max} in the field of view of the slit, computed with the streamer code. E_s is the actual peak electric field of the streamer head. Blue solid line: time evolution of the correction factor Γ with the estimated field derived from time-integrated OEs spatially integrated over the slit (equation (15)) and the steady-state equation (13). The open circle shows the time for which the estimated electric field is equal to E_s ($\Gamma = 1$).

experiments, pinholes could be used instead of slits to scan axially and radially the entire discharge domain. In Hoder *et al* (2010) a pinhole size down to 0.05 mm has been used to scan the discharge domain by means of the CCS technique. In this section we study the influence of time integration on the determination of the electric field from spatially resolved (i.e., windowed by a pinhole) OEs. Generally OE data directly available from laboratory experiments are at least line integrated over a line perpendicular to the propagation axis of the discharge, as given by equation (8). Then, in order to have the radial dependence of $A_k n_k$ from experimental data it is necessary to perform inverse Abel transformation on them. This may be a difficult task when the experimental data are noisy, therefore in this section we discuss the derivation of the electric field from both: (i) local and (ii) line-integrated OEs. The reference point is located on the axis of symmetry of the discharge in the middle of the computational domain ($z = L_d/2, r = 0$). Figure 7(*a*) compares the time evolution of E_{real}, the electric field on the axis of symmetry computed directly with the streamer code, $E_{e,inst}$, the electric field estimated using the steady-state equation (13) and local and instantaneous OEs, and $E_{e,ti}$, the electric field estimated using the steady-state equation (13) with time-integrated OEs according to equation (9). The peak value E_s of the electric field E_{real} for the reference point chosen ($z = L_d/2, r = 0$) is at time $t = 12.3$ ns (corresponding to figure 2). At this time, it is interesting to note that $E_{e,inst}$ reaches a value that is about twice the value of E_{real}. This result clearly shows that the steady-state condition is not fulfilled for air discharges at atmospheric pressure. Then, its direct use may overestimate the peak electric field by a factor of 2. The time evolution of $E_{e,inst}$ is the same as that of E_{real} with an increase, a peak value and a decrease, but the peak profile is broader. The half-width of the broadening is comparable to the effective lifetime of $N_2(C\,^3\Pi_u)$. After a sufficiently long time, $E_{e,inst}$ converges towards the actual electric field value when the non-stationary event is finished. However, as the electric field on the discharge axis behind the streamer head is too low for the excitation threshold of the emitting states $N_2(C\,^3\Pi_u)$ and $N_2^+(B\,^2\Sigma_u^+)$, the curve of $E_{e,inst}$ vanishes for $t > 13.5$ ns. The electric field $E_{e,ti}$ estimated using the steady-state equation (13) with time-integrated OEs has basically the same time evolution as that of $E_{e,inst}$. However, after the overshoot, the value of $E_{e,ti}$ converges towards a limit. The converged value of the derived electric field is E_e. This value takes into account the memory of the time-integrated estimated electric field profile. Then, for figure 7(*a*), we obtain a correction factor of $\Gamma = E_s/E_e = 1.28$. As in this section we have used local OEs on the axis of symmetry, and no volume integration, the Γ coefficient for the electric field on the discharge axis calculated for figure 7(*a*) can be considered as the correction factor for only Naidis' effect.

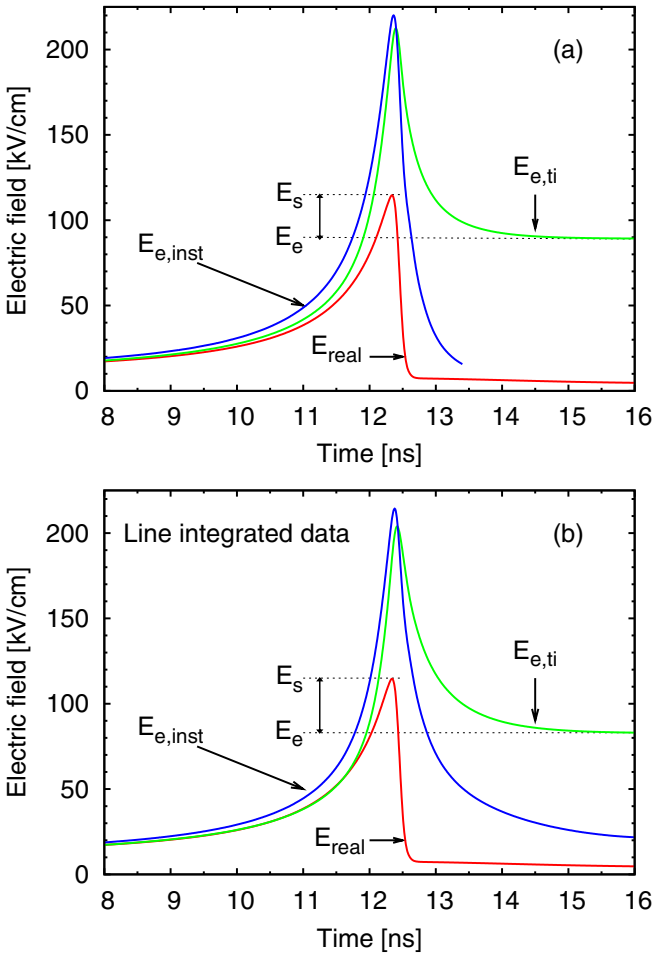

Figure 7. (a) Red solid line: time-dependent electric field E_{real} on the axis of symmetry in the middle of the computational domain ($z = L_{\mathrm{d}}/2, r = 0$), computed with the discharge code. E_{s} is the peak electric field of the streamer head. Blue solid line: time-dependent electric field $E_{\mathrm{e,inst}}$ estimated using the steady state equation (13) with local and instantaneous OEs. Green solid line: time-dependent electric field $E_{\mathrm{e,ti}}$ estimated using the steady-state equation (13) with local and time-integrated OEs. E_{e} is the converged value of the estimated value of electric field $E_{\mathrm{e,ti}}$. The correction factor $\Gamma = E_{\mathrm{s}}/E_{\mathrm{e}} = 1.28$ in this case. (b) Same as (a) except that for blue and green lines, the electric field is derived from line-integrated OEs. In this case, $\Gamma = 1.38$.

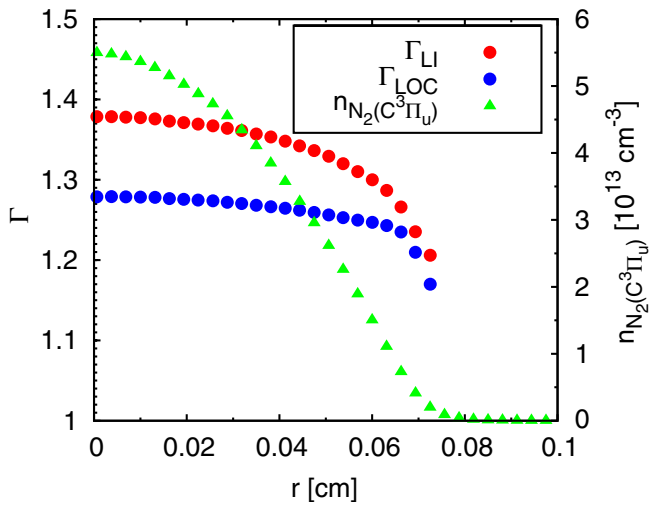

Figure 8. Radial distributions of correction factors and of the maximum density of $N_2(C\,^3\Pi_u)$ for pinholes located in the middle of the computational domain ($z = L_{\mathrm{d}}/2, r = 0$ to R_{d}). Red points: correction factor Γ_{LI} derived using the steady-state equation (13) and time- and line-integrated OEs. Blue points: correction factor Γ_{LOC} derived using the steady-state equation (13) and time-integrated and local OEs. Green points: maximum value of the density of $N_2(C\,^3\Pi_u)$ at the points $z = L_{\mathrm{d}}/2, r = 0$ to R_{d} during the whole streamer propagation in the computational domain.

To study the influence of line-integration on the derivation of the electric field, figure 7(b) compares the time evolution of E_{real}, the electric field on the axis of symmetry computed directly from the discharge code (same as in figure 7(a)), with the electric fields $E_{\mathrm{e,inst}}$ and $E_{\mathrm{e,ti}}$ estimated using the steady-state equation (13) and line-integrated (along an horizontal line of sight) OEs. As in figure 7(a), we note that the peak value of $E_{\mathrm{e,inst}}$ overestimates by a factor of about 2 the true value of the peak electric field in the streamer head E_{s}. The same time broadening as in figure 7(a) is observed, except that in this case for long times after the peak, the value of $E_{\mathrm{e,inst}}$ converges towards a value higher than the electric field E_{real} on the axis. As already mentioned, behind the streamer head, the electric field on the axis of the streamer channel is very low. However, in figure 7(b), we consider line-integrated OEs over a horizontal line. This line integration takes into account the radial contributions of the edges of the plasma where the electric field (and then the emission) is still significant. Then, the value of $E_{\mathrm{e,inst}}$ in figure 7(b) finally converges towards a value and does not vanish as in figure 7(a). It is also interesting to note that the electric field $E_{\mathrm{e,ti}}$ derived from the steady-state equation (13) and line-integrated and time-integrated OEs finally converge towards a limit as in figure 7(a). The converged value of the derived electric field is E_{e} and we note that this value is less than the one obtained in figure 7(a). For figure 7(b), the correction factor $\Gamma = E_{\mathrm{s}}/E_{\mathrm{e}} = 1.38$, that is higher than for figure 7(a). This result shows that the line integration increases the value of Γ.

Figure 8 presents the radial distribution of the correction factor $\Gamma = E_{\mathrm{s}}/E_{\mathrm{e}}$ for pinholes placed in the middle of the computational domain ($z = L_{\mathrm{d}}/2, r = 0$ to R_{d}) for time-integrated (i) local and (ii) line-integrated OEs. Results are presented together with the radial distribution of the maximum value of the density of $N_2(C\,^3\Pi_u)$. This radial profile of $N_2(C\,^3\Pi_u)$ is obtained by considering for each point ($z = L_{\mathrm{d}}/2, r = 0$ to R_{d}), the maximum value of the density of $N_2(C\,^3\Pi_u)$ during the whole time of propagation of the streamer in the computational domain. Then the radial extent of the maximum value of the density of $N_2(C\,^3\Pi_u)$ corresponds to the radial extent of the light intensity of the streamer. If we define the radius of the streamer as the radius where the density of $N_2(C\,^3\Pi_u)$ is 1/10 of its maximum value, we obtain in this case a radius of $R_{\mathrm{st}} = 0.07$ cm. Using local OEs, we note that the value of the Γ coefficient is maximum at $r = 0$ and equal to 1.28 (in agreement with figure 7(a)) and then slightly decreases as r increases to be equal to 1.24 for $r = R_{\mathrm{st}}$. This corresponds to variations of the Γ coefficient of less than 3% along the radial extension of the streamer. For line-integrated OEs, figure 8 shows that the decrease of Γ as r increases up to

R_{st} is more pronounced. The maximum value is 1.38 on the axis, in agreement with figure 7(*b*) and the minimum is 1.24 for $r = R_{st}$, which corresponds to a variation of about 10% along the radial extension of the streamer. Figure 8 shows that the values of the Γ coefficients determined using local and line-integrated OEs coincide for $r = R_{st}$. Indeed at this position, the line of integration is tangent to the streamer and the emitting regions taken into account in the line integration effectively become one single point and then the result of the line integration corresponds to the local calculation.

4.4. Einstein coefficients and quenching rate coefficients

The accurate knowledge of Einstein coefficients and quenching rates of $N_2(C\,^3\Pi_u)$ and $N_2^+(B\,^2\Sigma_u^+)$ states is essential for an accurate calculation of $N_2^+(B\,^2\Sigma_u^+)$ and $N_2(C\,^3\Pi_u)$ emission ratio. In the literature large discrepancies exist currently between the values measured by different authors (Paris *et al* 2005, Dilecce *et al* 2010, Valk *et al* 2010, and references therein). So far, in this work, we have used the coefficients reviewed by Liu and Pasko (2004) (given in table 1) and used by Celestin and Pasko (2010). Our objective was to use the same coefficients as in Celestin and Pasko (2010) to compare our results at ground pressure with their results at high altitudes. In order to explore the influence of the variation of Einstein coefficients and quenching rates on the correction factor Γ, we have performed simulations with two other sets of rate coefficients. These sets are recommended in Paris *et al* (2005) and Valk *et al* (2010), and listed in table 1.

We have verified that the correction factors Γ derived using the Einstein coefficients and quenching rates from Liu and Pasko (2004), Paris *et al* (2005) and Valk *et al* (2010) differ by less than 1%. In the preceding sections we have shown that the Γ coefficient is mostly a shape factor taking into account the geometry of the streamer head. As small changes in the kinetics of excited species have only weak influence on the structure of the streamer, they have also small influence on the value of Γ.

5. Conclusions

In this paper, we discuss different approaches to derive the electric field in positive streamer discharges in air at ground pressure based on the recordings of the emissions of the SPS and FNS. As a test-case, we have considered the propagation of a positive streamer in air at ground pressure and we have computed the spatio-temporal distributions of OEs and electric field in the discharge self-consistently. We have shown that the steady-state condition of emitting states $N_2^+(B\,^2\Sigma_u^+)$ and $N_2(C\,^3\Pi_u)$ is not fulfilled in air at ground pressure and then its use to determine the local and instantaneous peak electric field in the streamer head may overestimate this field by a factor of 2. However, when spatial and time-integrated OEs are considered, we have shown that it is possible to use the steady-state equation to accurately determine the peak electric field in an air discharge at atmospheric pressure. We have defined a correction factor $\Gamma = E_s/E_e$ (where E_e is the estimated electric field and E_s is the true peak electric field in the streamer head).

For instantaneous OEs integrated over the whole radiating plasma, we have shown that a correction factor of ∼1.4 has to be used. We have shown that this correction stems from (i) the shift between the location of the peak electric field and the maximum excitation rate for $N_2(C\,^3\Pi_u)$ and $N_2^+(B\,^2\Sigma_u^+)$ as proposed by Naidis (2009) and (ii) from the cylindrical geometry of the streamers as stated by Celestin and Pasko (2010).

For time-integrated OEs, we have shown that steady-state equation (13) can be used to derive the electric field in discharges if the time of integration is sufficiently long (i.e. at least longer than the longest characteristic lifetime of excited species) to have the time to collect all the light from the emitting zones of the streamer.

We have also studied the derivation of the electric field in air discharges at atmospheric pressure using OEs recorded using slits (i.e. a window with a small width but a sufficiently large radial extension to contain the total radial extension of the discharge). Our studies demonstrate that spatially integrated OEs over slits can be used with the steady-state equation (13) to determine the electric field. For this case we have calculated a correction factor ∼1.4. For OEs observed through pinholes, we have demonstrated that for local OEs, the Γ coefficient on the axis of the discharge is 1.28, corresponding to Naidis' effect alone. For line-integrated OEs, the Γ coefficient on the axis of the discharge is 1.38. The increase of the Γ factor by taking into account the line integration clearly shows that the correction factor is mostly a shape factor of the geometry of the streamer head.

We have studied the radial distribution of the coefficient Γ when pinholes are used. For local and line-integrated OEs, we have shown that the highest value of Γ is obtained on the discharge axis and the Γ coefficient decreases for larger radius. For local OEs, we have shown that the Γ coefficient varies in the range [1.24, 1.28] along the radius of the streamer, which corresponds to a 3% variation in the radial direction. For line-integrated OEs, the radial variation of Γ has a broader range [1.24, 1.38], which corresponds to a 10% variation in the radial direction.

Finally, the influence of the use of different sets of Einstein coefficients and quenching rates of excited states has been studied. As the Γ coefficient is mostly a shape factor of the geometry of the streamer head, small changes in the kinetics of excited species, which have only weak influence on the structure of the streamer, have negligible influence on the value of Γ.

Acknowledgments

This work was supported by the Agence Nationale de la Recherche under project PREPA (Grant No ANR-09-BLAN-0043-03), Z Bonaventura is also grateful to the Ministry of Education, Youth and Sports of the Czech Republic under project CZ.1.05/2.1.00/03.0086 and project MSM 0021622411. Participation of S Celestin and V P Pasko was supported by the United States National Science

Foundation under the AGS 0734083 grant to Penn State University.

References

Bourdon A, Pasko V P, Liu N Y, Celestin S, Segur P and Marode E 2007 Efficient models for photoionization produced by non-thermal gas discharges in air based on radiative transfer and the Helmholtz equations *Plasma Sources Sci. Technol.* **16** 656–78

Bourdon A, Bonaventura Z and Celestin S 2010 Influence of the pre-ionization background and simulation of the optical emission of a streamer discharge in preheated air at atmospheric pressure between two point electrodes *Plasma Sources Sci. Technol.* **19** 034012

Celestin S and Pasko V P 2010 Effects of spatial non-uniformity of streamer discharges on spectroscopic diagnostics of peak electric fields in transient luminous events *Geophys. Res. Lett.* **37** L07804

Demmel J W, Eisenstat S C, Gilbert J R, Li X S and Liu J W H 1999a A supernodal approach to sparse partial pivoting *SIAM J. Matrix Anal. Appl.* **20** 720–55

Demmel J W, Gilbert J R and Li X S 1999b An asynchronous parallel supernodal algorithm for sparse gaussian elimination *SIAM J. Matrix Anal. Appl.* **20** 915–52

Dilecce G, Ambrico P F and De Benedictis S 2010 On the collision quenching of $N_2^+(B\,^2\Sigma_u^+, v = 0)$ by N_2 and O_2 and its influence on the measurement of E/N by intensity ratio of nitrogen spectral bands *J. Phys D: Appl. Phys.* **43** 195201

Gallimberti I, Hepworth J K and Klewe R C 1974 Spectroscopic investigation of impulse corona discharges *J. Phys. D: Appl. Phys.* **7** 880–99

Hoder T, Šíra M, Kozlov K V and Wagner H-E 2008 Investigation of the coplanar barrier discharge in synthetic air at atmospheric pressure by cross-correlation spectroscopy *J. Phys. D: Appl. Phys.* **41** 035212

Hoder T, Brandenburg R, Basner R, Weltmann K-D, Kozlov K V and Wagner H-E 2010 A comparative study of three different types of barrier discharges in air at atmospheric pressure by cross-correlation spectroscopy *J. Phys. D: Appl. Phys.* **43** 124009

Kozlov K, Wagner H, Brandenburg R and Michel P 2001 Spatio-temporally resolved spectroscopic diagnostics of the barrier discharge in air at atmospheric pressure *J. Phys. D: Appl. Phys.* **34** 3164–76

Kulikovsky A A 1995 A more accurate Scharfetter–Gummel algorithm of electron transport for semiconductor and gas discharge simulation *J. Comput. Phys.* **119** 149–55

Kuo C, Hsu R, Chen A, Su H, Lee L, Mende S, Frey H, Fukunishi H and Takahashi Y 2005 Electric fields and electron energies inferred from the ISUAL recorded sprites *Geophys. Res. Lett.* **32** L19103

Kuo C-L *et al* 2009 Discharge processes, electric field, and electron energy in ISUAL-recorded gigantic jets *J. Geophys. Res.—Space Phys.* **114** A04314

Liu N 2010 Model of sprite luminous trail caused by increasing streamer current *Geophys. Res. Lett.* **37** L04102

Liu N and Pasko V 2004 Effects of photoionization on propagation and branching of positive and negative streamers in sprites *J. Geophys. Res.—Space Phys.* **109** A04301

Liu N, Celestin S, Bourdon A, Pasko V P, Segur P and Marode E 2007 Application of photoionization models based on radiative transfer and the Helmholtz equations to studies of streamers in weak electric fields *Appl. Phys. Lett.* **91** 211501

Liu N Y and Pasko V P 2006 Effects of photoionization on similarity properties of streamers at various pressures in air *J. Phys. D: Appl. Phys.* **39** 327–34

Liu N Y, Pasko V P, Adams K, Stenbaek-Nielsen H C and McHarg M G 2009 Comparison of acceleration, expansion, and brightness of sprite streamers obtained from modeling and high-speed video observations *J. Geophys. Res.* **114** A00E03

Morrow R and Lowke J J 1997 Streamer propagation in air *J. Phys. D: Appl. Phys.* **30** 614–27

Naidis G V 2009 Positive and negative streamers in air: velocity–diameter relation *Phys. Rev.* E **79** 057401

Pancheshnyi S, Starikovskaia S and Starikovskii A 1998 Measurements of rate constants of the $N_2(C\,^3\Pi_u, v' = 0)$ and $N_2^+(B\,^2\Sigma_u^+, v' = 0)$ deactivation by N_2, O_2 H_2, CO and H_2 O molecules in afterglow of the nanosecond discharge *Chem. Phys. Lett.* **294** 523–7

Pancheshnyi S, Sobakin S, Starikovskaya S and Starikovskii A 2000 Discharge dynamics and the production of active particles in a cathode-directed streamer *Plasma Phys. Rep.* **26** 1054–65

Paris P, Aints M, Valk F, Plank T, Haljaste A, Kozlov K and Wagner H 2005 Intensity ratio of spectral bands of nitrogen as a measure of electric field strength in plasmas *J. Phys. D: Appl. Phys.* **38** 3894–9

Pasko V P, Inan U S, Bell T F and Taranenko Y N 1997 Sprites produced by quasi-electrostatic heating and ionization in the lower ionosphere *J. Geophys. Res.* **102** 4529–61

Starikovskaia S M, Allegraud K, Guaitella O and Rousseau A 2010 On electric field measurements in surface dielectric barrier discharge *J. Phys. D: Appl. Phys.* **43** 124007

Valk F, Aints M, Paris P, Plank T, Maksimov J and Tamm A 2010 Measurement of collisional quenching rate of nitrogen states $N_2(C\,^3\Pi_u, v = 0)$ and $N_2^+(B\,^2\Sigma_g^+, v' = 0)$ *J. Phys. D: Appl. Phys.* **43** 385202